IEEE Access
Multidisciplinary | Rapid Review | Open Access Journal

Received May 10, 2022, accepted June 2, 2022, date of publication June 14, 2022, date of current version June 21, 2022.

Digital Object Identifier 10.1109/ACCESS.2022.3183004

Spatial Propagation Law of Magnetic Memory Signals Detected by Using Magnetic Tomography Method

LINLIN LIU[1,2], LIJIAN YANG[1], AND SONGWEI GAO[1]
[1]School of Information Science and Engineering, Shenyang University of Technology, Shenyang 110870, China
[2]School of Information and Control Engineering, Liaoning Petrochemical University, Fushun 113001, China

Corresponding author: Linlin Liu (dl198182@163.com)

ABSTRACT Magnetic tomography is a new and nondestructive testing technology based on the metal magnetic memory method, which can perform noncontact testing outside a pipeline. To identify the type of defect from the characteristics of the magnetic field signal detected by this method, we performed basic research on the propagation mechanism of a magnetic memory signal outside the pipe. In this paper, a magnetic field model of the stress concentration zone was first discussed based on the magnetic dipole theory. A 3-D formulation of the spatial propagation of the magnetic memory signals detected by the magnetic tomographic method was built, based on the Biot–Savart law and the magnetic vector potential. The reliability of the model was verified by comparing the field testing signal with the model-calculated values. The model can well describe the propagation law of the magnetic memory signal for the stress concentration zone generated on the inner wall of a pipeline.

INDEX TERMS Magnetic tomographic method, law of magnetic field propagation, stress concentration zone, magnetic anisotropy, magnetic dipole.

I. INTRODUCTION

Metal magnetic memory detection technology [1]–[4] has been used to detect defects and discontinuous parts in pipelines in recent years. A magnetic anomaly is formed on the stress concentration zone after a pipeline is magnetized. The risk can be effectively evaluated and prevented by determining the type and location of defects via analyzing the characteristics of the residual magnetic leak field. However, many oil and gas pipelines are not easy to implement for internal inspection due to the laying environment and the pipeline structure [5].

The magnetic tomography method (MTM) was proposed by Russian experts, and is a nondestructive detection method for magnetic memory signals produced by the natural magnetization of ferromagnetic materials in geomagnetic environments [6], [7]. The method has been widely used to inspect subsea and buried pipelines in recent years. Using the MTM to examine subsea pipelines in cold regions and the Arctic can not only identify defects remotely but also record mechanical stress levels based on actual loads. It is claimed that risk management in the event of localized corrosion, stress cracking or loss of stability of the submerged pipeline in the free-span area can be carried out in parallel with the inspection [8], [9]. The the feasibility and validity were evaluated by using the MTM to inspect girth welds on buried pipes [10].

The essence of the MTM lies in the correlation between the magnetic field parameters of the pipe and the level of mechanical stress, which has been assessed by many scholars through simulation experiments and based on metal magnetostriction and magnetic field stress theory [6], [9]. An image-only relationship between stress and magnetization was proposed based on the magnetic dipole model, and a magnetic-force coupling model based on the Z-L model for the stress concentration zone was established. The model did not determine the 3-D magnetic field distribution outside the pipeline [11]. A gradient model based on a ground leakage magnetic field (GLMF) was proposed to determine the stress concentration zone by the change in the gradient modulus [12]. However, the prediction level would be higher than the GLMF because the model did not consider the effect of the magnetic path in the magnetized zone around the pipeline. An AMR sensor array [13] was designed after evaluating the factor of the perturbation of the magnetic field surrounding

The associate editor coordinating the review of this manuscript and approving it for publication was Wuliang Yin.

the pipeline, and the accuracy was verified by an experimental study of a flat-bottom defect. At present, MTM detection is performed by analyzing the gradient changes in the detection signal to discern the stress concentration zone, and the detection result has a high error rate. Therefore, a systematic study of the quantified relationship between the magnetic field of the stress concentration zone and the MTM detection signal can provide a scientific basis for the mechanism of the MTM. At the same time, this research can promote the scientific application of the MTM. This is also the purpose of this paper.

In this paper, a spatial propagation model of magnetic memory signals is proposed, which can quantitatively explain the relationship between the magnetic field of the stress concentration zone and the magnetic signal detected by the MTM. The distribution of the stress concentration zone magnetic signal on a pipeline and in the air based on magnetic dipole theory and the Biot–Savart law is determined. The distribution characteristics are determined by a numerical analysis of the model. Moreover, the validity of the model proposed in this paper is verified in engineering experiments.

This paper is composed of six sections. In Section 2, we introduce the basic principle of magnetic tomography detection in detail. This is followed by Section 3, where we determine equivalent model of the stress concentration zone and the spatial propagation model of the MTM. In Section 4, we analyze the spatial propagation model using a numerical method. After that, by comparing the theoretical results and experimental results, the effectiveness of the theoretical model is verified in Section 5. Section 6 offers the conclusion of this paper.

II. PHYSICAL PRINCIPLE OF MAGNETIC TOMOGRAPHY METHOD

A. MAGNETIC TOMOGRAPHY DETECTION

A buried oil and natural gas pipeline is affected by the geomagnetic field, and magnetic memory signals are formed on ferromagnetic materials because of the Villari effect. These magnetic domains are subject to displacement or irreversible rearrangement, which manifests as an abnormality in the magnetic signal when there is a local stress concentration on the pipe. The distorted magnetic signal remains in the ferromagnetic material after the charge is removed.

The magnetic memory signal can be measured by an MTM detector due to the propagation of magnetic field from the pipeline through the soil to the ground surface. A schematic diagram of MTM detection is shown in Figure 1. The magnetic memory signal is measured with a handheld magnetometer [14] that by a staff member walking axially along the buried pipeline. By analyzing the detection signal, the stress concentration zone is discriminated by the gradient change of the magnetic memory signal.

B. THEORETICAL MODEL

The magnetic configuration of a ferromagnetic pipeline is a multiaxial magnetic crystal structure. The magnetic domain

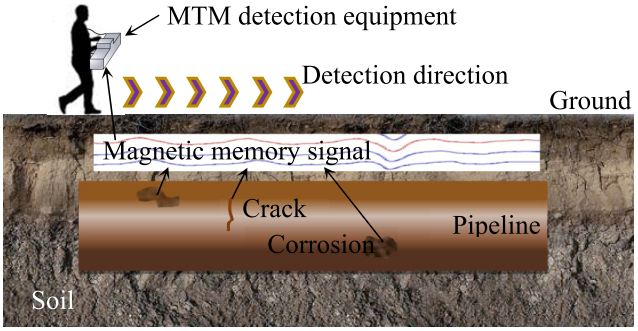

FIGURE 1. Schematic diagram of MTM.

structure is altered, under the action of a magnetic field. Therefore, the magnetic field strength is different in different directions of the crystal structure. The distribution characteristics of the magnetic field on the pipeline show anisotropy.

In an anisotropic magnetic medium, the magnetic vector potential [15] is expressed as follows:

$$\mathrm{A}_i = \frac{1}{4\pi\sqrt{|\mu_{mn}|}} \sum_{i=1}^{3} \Delta_{im} \int \frac{\mathrm{j}_l d\Omega}{\left[\sum_{j=1}^{3}\sum_{k=1}^{3} (\mu jk)^{-1} R_j R_k\right]^{\frac{1}{2}}}, \quad i = 1, 2, 3 \tag{1}$$

where $|\mu_{mn}|$ is the determinant of the tensor permeability μ_{mn} $(m, n= 1, 2, 3)$, Δ_{im} is the algebraic cofactor of permeability $\mu_{\theta l}$, j_l is the free current density, R_j is the axial component of the vector diameter from the magnetic source to any point in space and $d\Omega$ is the integral volume element.

If the expression of the magnetic vector potential $\mathbf{A}$ is known, then the magnetic flux intensity $\mathbf{B}$ can be determined by Equation (2), as follows:

$$\mathbf{B} = \nabla \times \mathbf{A} \tag{2}$$

The relationship between the magnetic vector potential $\mathbf{A}$ and the free current density $\mathbf{J}$ can be described as follows:

$$\nabla \times \left(\boldsymbol{\mu}^{-1} \cdot \nabla \times \mathbf{A}\right) = \mathbf{J} \tag{3}$$

Thus, we deduct the Biot–Savart law [16] in the anisotropic magnetic medium from (2) and (3), as follows:

$$\mathbf{B} = \frac{1}{4\pi} \int \frac{\mathbf{J} d\Omega \times \sum_{j=1}^{3}\sum_{k=1}^{3} \left(\mu_{jk}\right)^{-1} R_j \mathbf{e_j}}{\left[\sum_{j=1}^{3}\sum_{k=1}^{3} \left(\mu_{jk}\right)^{-1} R_j R_k\right]^{3/2}} \tag{4}$$

III. SPATIAL PROPAGATION MODEL OF MAGNETIC TOMOGRAPHY METHOD

To simplify the analysis, the research in this paper is based on the assumption that the stress concentration zone is located directly above the inner wall of the pipeline, without considering the influence of the geological environment. The magnetic field model of the stress concentration zone is

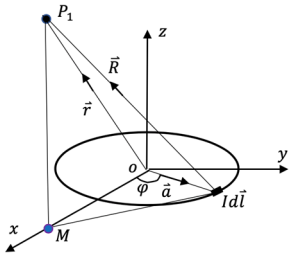

FIGURE 2. Magnetic dipole model.

established by a magnetic dipole model. The magnetic field generated by the current-carrying coil is considered to be a magnetic dipole field [17], [18]. The current-carrying coil is set on the inner wall of the pipeline, and P_1 is any point on the pipe wall. P is any point in the outer space of the pipeline, where the measurement sensor is located in Figure 2. The radius of the current carrying coil is much smaller than the radius of the pipeline. Thus, the pipe wall can be regarded as a plane in comparison with the current-carrying coil.

I is the intensity of the current of the current carrying coil [19], and **a** is the radius of the coil. O is the center of the coil, and coincides with the origin of the Cartesian coordinate system. The y-axis is parallel to the axis of the cylindrical cavity of the magnetic material and located in the inner wall of the pipe. The x axis is perpendicular to the internal diameter of the cylindrical cavity, and the z-axis is perpendicular to the cylindrical cavity. H is the vertical distance between P_1 and the Oxy plane, L is the length of **OM**, **r**is the vector diameter from O and P_1, and **R** is the vector diameter from the current element **Idl** to P_1.

For the direction of magnetic flux intensity, only a few crystal axes are the same as the magnetic source itself, according to the symmetry law of cubic crystals of anisotropic magnetic materials [20]. These few crystal axes are the main axes of magnetic anisotropy. To simplify the analysis, the case in which the three linear and orthogonal principal axes of the magnetic anisotropic medium coincide with the coordinate axes of the Cartesian coordinate system is considered. Thus, x', y', and z' are the three main axes of the magnetic anisotropic material, and they coincide with the origin of the coordinate axes of the current carrying coil. In this case, only the main diagonal permeability component of the permeability tensor matrix is nonzero, and the permeability μ_{mn} can be expressed as follows:

$$[\mu_{mn}] = \begin{bmatrix} \mu_{11} & 0 & 0 \\ 0 & \mu_{22} & 0 \\ 0 & 0 & \mu_{33} \end{bmatrix} \tag{5}$$

The conversion relationship between the volume distribution and line distribution of the free current density is as follows:

$$\mathbf{J}d\Omega = \mathbf{Idl} \tag{6}$$

By substituting (6) into (4), the magnetic flux intensity of P_1on magnetic anisotropic materials can be expressed as follows:

$$\mathbf{B} = \frac{\boldsymbol{\mu}'''}{4\pi}\int \frac{\mathbf{Idl}\times\mathbf{R}}{\left(\frac{R_x^2}{\mu_{xx}}+\frac{R_y^2}{\mu_{yy}}+\frac{R_z^2}{\mu_{zz}}\right)^{3/2}} \tag{7}$$

where $\boldsymbol{\mu}''' = (\mu_{xx}/(\mu_{yy}\mu_{zz}))^{1/2}\mathbf{e_x}\mathbf{e_x}+(\mu_{yy}/(\mu_{xx}\mu_{zz}))^{1/2}\mathbf{e_y}\mathbf{e_y}+(\mu_{zz}/(\mu_{xx}\mu_{yy}))^{1/2}\mathbf{e_z}\mathbf{e_z}$.

The angle between $\mathrm{Id}\vec{l}$ and x-axis is assumed to be φ, and the angle between **r** and O is θ.

$$\mathbf{I} = a\cos\varphi\mathbf{e_x} + a\sin\varphi\mathbf{e_y} \tag{8}$$

$$\mathbf{Idl} = a\mathrm{I}(-\sin\varphi\mathbf{e_x}+\cos\varphi\mathbf{e_y})\mathrm{d}\varphi \tag{9}$$

$$\mathbf{R} = (L - a\cos\varphi)\,\mathbf{e_x} - a\sin\mathbf{e_y} + H\mathbf{e_z} \tag{10}$$

$$\mathbf{R} = \mathbf{Re_x}+\mathbf{Re_y}+\mathbf{Re_z} \tag{11}$$

where $R_\mathrm{x} = L - a\cos\varphi$, $R_\mathrm{y} = -a\sin\varphi$, $R_\mathrm{z} = H$.

Substituting (9) and (10) into (7), the following equation (12) is obtained:

$$dB = \frac{\boldsymbol{\mu}'''}{4\pi}\int \frac{\mathbf{Idl}\times\mathbf{R}}{\left(\frac{R_x^2}{\mu_{xx}}+\frac{R_y^2}{\mu_{yy}}+\frac{R_z^2}{\mu_{zz}}\right)^{3/2}} = \frac{aI\boldsymbol{\mu}'''}{4\pi}\left\{\frac{H\cos\varphi\mathbf{e_x} + H\sin\varphi\mathbf{e_y} + (a - L\cos\varphi)\mathbf{e_z}}{\left[\frac{(L-a\cos\varphi)^2}{\mu_{xx}} + \frac{a^2\sin^2\varphi}{\mu_{yy}} + \frac{H^2}{\mu_{zz}}\right]^{3/2}}\right\} \tag{12}$$

B is given in terms of the integral of (12). Therefore, the three components of the magnetic flux intensity of the magnetic field of the stress concentration zone at any point [21] of the pipeline can be expressed as follows:

$$\mathrm{B}_{1x} = \frac{aI}{4\pi}\sqrt{\frac{\mu_{xx}}{\mu_{yy}\mu_{zz}}}\int_0^{2\pi}\frac{H\cos\varphi}{\left[\frac{(L-a\cos\varphi)^2}{\mu_{xx}}+\frac{a^2\sin^2\varphi}{\mu_{yy}}+\frac{H^2}{\mu_{zz}}\right]^{3/2}}d\varphi \tag{13}$$

$$\mathrm{B}_{1y} = \frac{aI}{4\pi}\sqrt{\frac{\mu_{yy}}{\mu_{zz}\mu_{xx}}}\int_0^{2\pi}\frac{H\sin\varphi}{\left[\frac{(L-a\cos\varphi)^2}{\mu_{xx}}+\frac{a^2\sin^2\varphi}{\mu_{yy}}+\frac{H^2}{\mu_{zz}}\right]^{3/2}}d\varphi \tag{14}$$

$$\mathrm{B}_{1z} = \frac{aI}{4\pi}\sqrt{\frac{\mu_{zz}}{\mu_{xx}\mu_{yy}}}\int_0^{2\pi}\frac{\mathrm{a} - L\cos\varphi}{\left[\frac{(L-a\cos\varphi)^2}{\mu_{xx}}+\frac{a^2\sin^2\varphi}{\mu_{yy}}+\frac{H^2}{\mu_{zz}}\right]^{3/2}}d\varphi \tag{15}$$

The magnetic memory signal propagates from the pipe to the space outside. The pipe and the outer space of the pipe are two different propagation media. Thus, the magnetic field intensity changes when the magnetic field line passes through different media [22], and the propagation relationship meets the Dirichlet boundary condition.

According to the boundary connection condition of static magnetism and the Gaussian theorem of $\nabla \cdot \mathbf{B} = \mathbf{0}$, the normal component of magnetic induction intensity is continuous at the boundary between the pipe and the air, as follows:

$$B_{1n} = B_{2n} \tag{16}$$

Thus, the normal component of the magnetic flux intensity of the stress concentration zone outside the pipeline is as follows:

$$\mathrm{B}_{2n} = \frac{aI}{4\pi}\sqrt{\frac{\mu_{zz}}{\mu_{xx}\mu_{yy}}}\int_0^{2\pi}\frac{\mathrm{a} - L\cos\varphi}{\left[\frac{(L-a\cos\varphi)^2}{\mu_{xx}}+\frac{a^2\sin^2\varphi}{\mu_{yy}}+\frac{H^2}{\mu_{zz}}\right]^{3/2}}d\varphi \tag{17}$$

According to the nondispersive of magnetic field [23] and the Ampere loop theorem, the relationship between magnetic flux intensity B and current intensity I can be expressed as follows:

$$\oint_L \mathbf{B}\cdot dl = \mu_0 \sum\nolimits_{\mathrm{Lin}} I \tag{18}$$

Under magnetostatic conditions, no conducted current exists on either side of the pipe wall or the boundary of the space environment. Therefore, the continuity relationship of the tangential component of the magnetic field intensity between different propagation media is as follows:

$$H_{1t} = H_{2t} \tag{19}$$

According to the refraction relation of the magnetic induction line at the medium interface and the electromagnetic property, Equation (20) is:

$$B_s = \sum\nolimits_{i=1}^{3} \mu_{si} H_i, \quad s = 1, 2, 3 \tag{20}$$

The relationship among the tangential components of magnetic flux intensity between different media is obtained as follows:

$$B_{2t} = \frac{\mu_2}{\mu_1} B_{1t} \tag{21}$$

where B_{2t} is the tangential component in the air, B_{1t} is the tangential component on the pipe, μ_2 is the permeability of free space and μ_1 is the permeability of the pipe material.

$$\frac{\mu_2}{\mu_1} = \mu_r \left[\mu_{mn}\right]^{-1} = \mu_r \frac{[\mu_{mn}]^*}{|\mu_{mn}|} \tag{22}$$

By calculating the adjoint matrix and determinant, (22) can be written as (23):

$$\frac{\mu_2}{\mu_1} = \mu_r \begin{bmatrix} 1/\mu_{xx} & 0 & 0 \\ 0 & 1/\mu_{yy} & 0 \\ 0 & 0 & 1/\mu_{zz} \end{bmatrix} \tag{23}$$

Hence, the tangential component of the magnetic flux intensity at any point outside the pipe is obtained as follows:

$$B_{2t} = \mu_r \left[\mu_{mn}\right]^{-1} \frac{aI}{4\pi}\sqrt{\frac{\mu_{xx}}{\mu_{yy}\mu_{zz}}} \tag{24}$$

$$\int_0^{2\pi}\frac{H\cos\varphi}{\left[\frac{(L-a\cos\varphi)^2}{\mu_{xx}}+\frac{a^2\sin^2\varphi}{\mu_{yy}}+\frac{H^2}{\mu_{zz}}\right]^{3/2}}d\varphi \tag{25}$$

where $[\mu_{mn}]^{-1} = \boldsymbol{\mu}^{-1} = \mu_{xx}^{-1}\mathbf{e_x}\mathbf{e_x} + \mu_{yy}^{-1}\mathbf{e_y}\mathbf{e_y} + \mu_{zz}^{-1}\mathbf{e_z}\mathbf{e_z}$.

IV. MODEL CALCULATION AND ANALYSIS

A. PROPAGATION ON PIPELINE WALL

This section presents the numerical calculation of the model that corresponds to the magnetic flux intensity on the pipeline. As described in Sections 2 and 3, the pipeline distribution model parameters are as follows: $a = 0.05$ m, $I = 1$ A. The magnetic flux intensity of different thicknesses on the outer wall is calculated as shown in Table 1.

TABLE 1. Peak value of magnetic flux intensity.

Thickness (mm)	Peak value of tangential component (nT)	Peak value of normal component (nT)
8	5531	5534
11.5	3750	3761
12	3582	3584
15	2791	2793

The magnetic flux intensity on the outer wall of the pipeline decreases gradually as the thickness value increases, as shown in Figure 3. The peak value decreases by 47.8% when the thickness decreases from 15 mm to 8 mm. This finding is consistent with the conclusion of the relationship between the detection height and the magnetic signal strength obtained by previous experiments [24]. A similar trend of distribution exists for all magnetic flux intensities with increasing thickness increases.

B. PROPAGATION OUTSIDE PIPELINE

This section discusses the numerical calculation of the space propagation model of the magnetic memory signal. The parameter setting is the same as that in the previous section. Figure 4 shows the tangential and normal components of the magnetic flux intensity along the x-axis for the pipeline with different lifting values.

Figure 4(a) indicates that tangential component curves cross zero, which is the same trend as the curves shown in Figure 3. The absolute value of the tangential component of the spatial magnetic flux intensity of the magnetic memory signal decreases significantly with increasing measuring height compared with the same measuring point of the axial direction. Figure 4(b) shows that the normal component is symmetrical with a peak on the symmetry axis. The normal component of the magnetic flux intensity decreases rapidly with increasing measurement points.

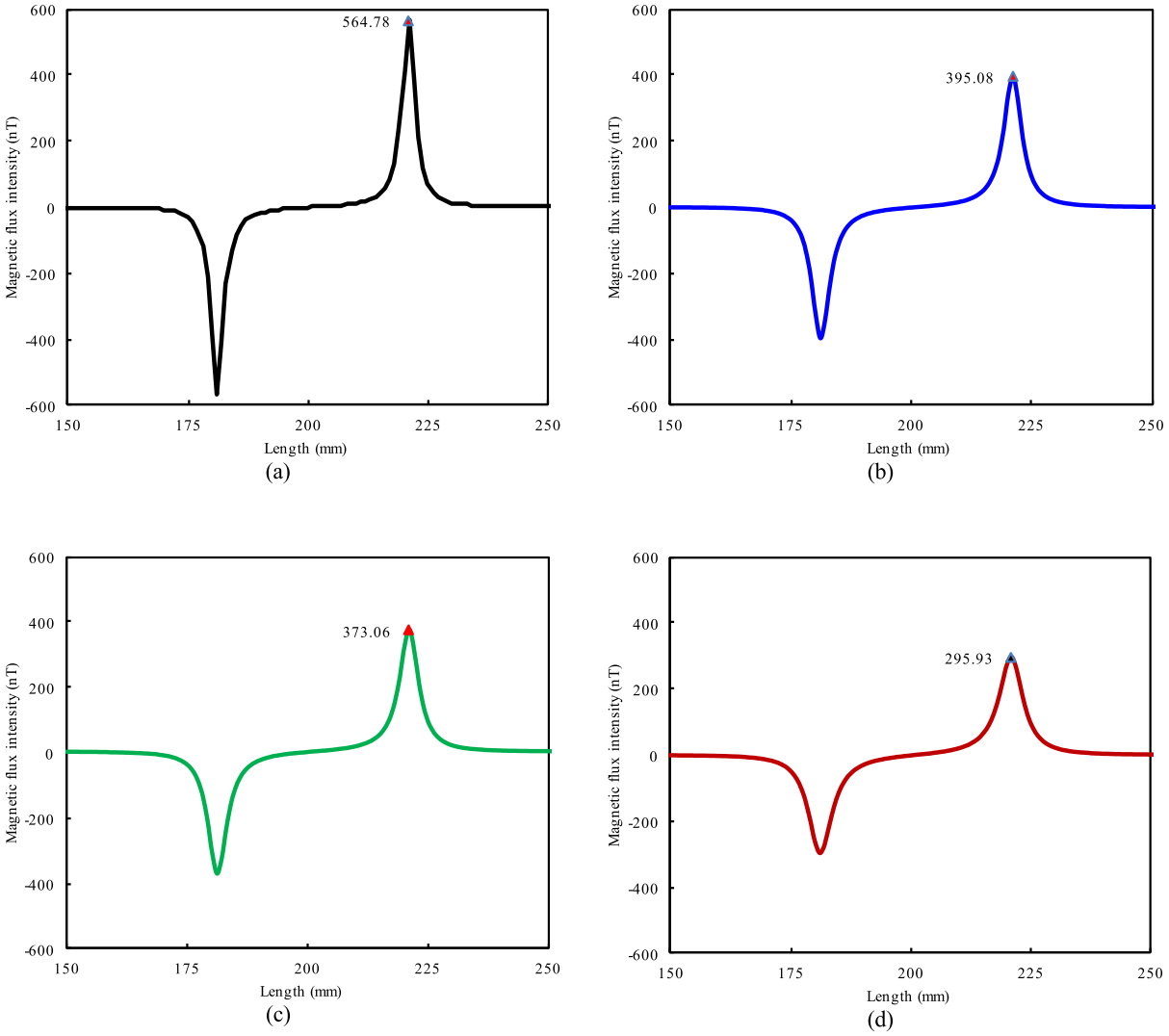

FIGURE 3. Curves of horizontal components of magnetic flux intensity of four pipeline thicknesses (a) the thickness is 8 mm (b) the thickness is 11.5 mm (c) the thickness is 12 mm (d) the thickness is 15 mm.

Analyzing the curves, the characteristics of the spatial propagation law of the MTM are determined. Under the action of a weak magnetic field, a magnetic field distortion signal is generated in the stress concentration zone, which is represented by the prominent peak value. When the measurement position is far greater than the thickness of the pipeline, the peak value trend of the distorted magnetic flux intensity can be detected, which also verifies the effectiveness of the MTM.

V. EXPERIMENTS AND ANALYSIS

A. EXPERIMENTAL METHOD

To verify the validity of the model proposed in this paper, a pipeline sample was tested on location. Testing was conducted using a current carrying coil, a detection sensor, an upper computer, and a data processing system, as shown in Figure 5.

The test object is an X80 nonweld pipe fitting, with a length of 5 m. Its inner diameter is 450 mm, and its wall thickness is 20 mm. The current-carrying coil was placed on the inner wall of the pipe, the radius of the coil was 50 mm, and the direct current intensity was 1 A. The center of the coil was considered the origin of the coordinate system. The detection sensor was fixed on a frame made of nonmagnetic material that was moved at a uniform speed outside the pipe to measure the magnetic flux intensity.

Before detection, the geomagnetic field distribution in the test area was measured to isolate valid data for later processing. The area to be measured was far away from other magnetic materials to ensure that the test results were not affected by other magnetic field components.

B. RESULTS AND ANALYSIS

The spatial propagation magnetic signals of the stress concentration region magnetic signal are shown in Figure 6 and Figure 7. The lifting values were separately 50, 100, and 150 mm, and the center of the current-carrying coil was located 100 mm from the origin of the detection axially.

The magnetic anomaly appears where the current-carrying coil is located. As shown in Figure 6, the tangential curve

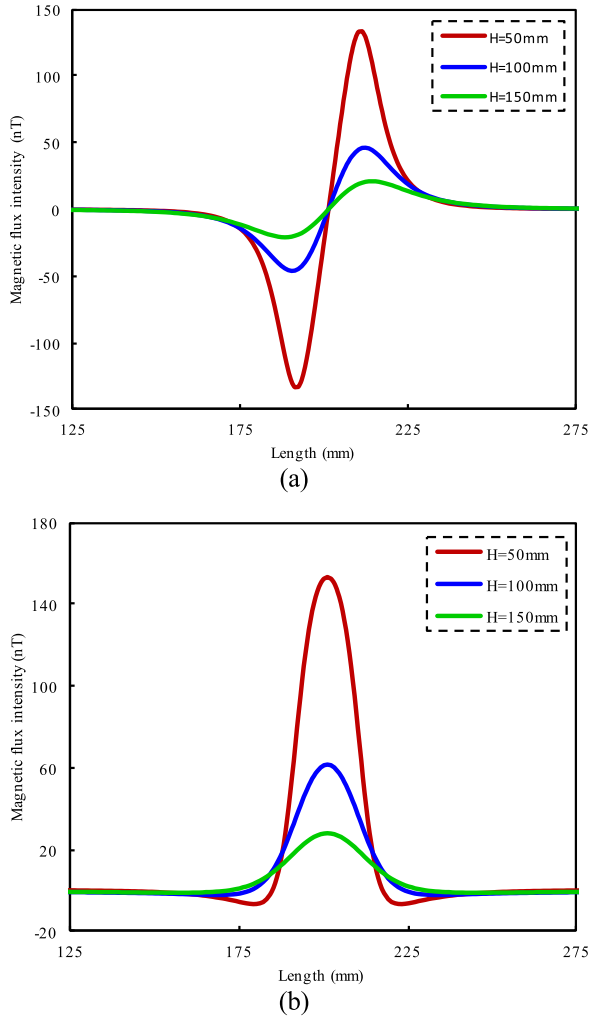

FIGURE 4. (a) The tangential component of magnetic flux intensity and (b) the normal component of magnetic flux intensity at different lifting values H when the length L is varied in the short length range.

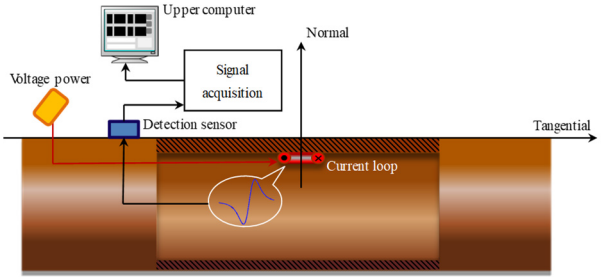

FIGURE 5. Schematic diagram of the test method.

of magnetic flux intensity passes through the zero point, and has a peak and trough. The normal component has a peak in Figure 7. As the propagation distance increases, the intensity of the magnetic signal decreases. There is a difference between the theoretical values and testing values due to a remnant magnetism in the pipeline; however, the distribution trend has not changed significantly.

The normal magnetic flux density curves of the actual testing and theoretical calculation above the pipeline are shown in Figure 8 when the lift-off is 150 mm. A peak value

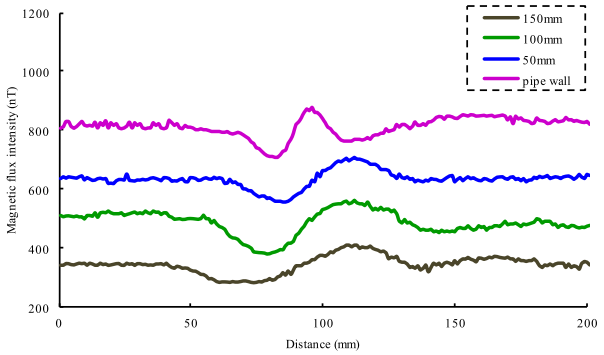

FIGURE 6. Tangential curves of testing value at H = 50 mm, 100 mm and 150 mm.

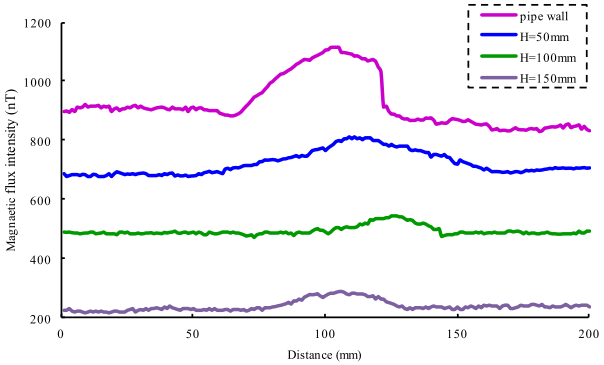

FIGURE 7. Normal curves of testing value at H = 50 mm, 100 mm and 150 mm.

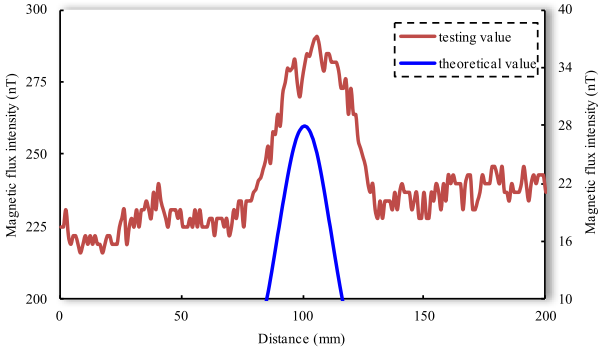

FIGURE 8. The normal magnetic flux density curve of the theoretical calculation and actual testing when H = 50mm.

point appears at approximately 105 mm of the axial position above the pipeline and its value is 290.3 nT for testing. The current-carrying coil is set in the pipeline at 100 mm from the axial position. The peak value error between the theoretical calculation and testing is 5%. The relative errors for different lift-off are separately 85.1% for H = 5 mm, 94.2% for H = 10 mm and 95.6% for H = 15 mm. The maximum relative error appears when the lift-off is 15 mm. The deviation between the peak point and the center of the current-carrying coil is 5 mm. The deviation is because the detection signal is a weak magnetic signal, which is susceptible to shocks and interference factors.

The overall trend of the magnetic field and the position of the stress concentration region outside the pipeline are basically consistent with the magnetic distribution of the

current-carrying coil. According to the analysis, the model is valid for calculating the position and magnetic distribution of the stress concentration region.

VI. CONCLUSION

MTM technology has a broad application prospects in subsea and buried pipeline detection. However, there is no scientific basis for the relationship between a stress concentration region characteristic and the magnetic signal detected by using the MTM. The spatial propagation model presented in this paper can well describe the location and characteristics of a stress concentration region generated on the inner wall of a pipeline. The spatial propagation law of magnetic memory signals is concluded as follows:

1) The magnetic memory signal can be detected outside a pipeline. The magnetic flux intensity of the signal attenuates faster in a pipeline than in the air. The relative error increases as the detection height increases.
2) The magnetic flux density decays significantly as the propagation distance increases, indicating that the detection range of the MTM is related to the physical characteristics of the covering materials.
3) The characteristic and the location of the magnetic memory signal detected outside a pipeline are consistent with the stress concentration region.

MTM detection has been applied in many projects, and the effective distance of vertical measurement and the size and the type of detectable defects remain to be explored in the future.

REFERENCES

[1] A. A. Dubov, "Diagnostics of metal items and equipment by means of metal magnetic memory," in *Proc. NDT U.K. Corrosion Conf.*, Poole, U.K., 1999, pp. 287–293.
[2] J. L. Ren, "Magnetization," in *Metal Magnetic Memory Testing Technique*, 1st ed. Beijing, China: CEPP, 2000, pp. 5–10.
[3] W. C. Zhong, "Theoretical fundamentals of the metal magnetic memory: Spontaneous magnetization of ferromagnetic materials by elastic-plastic strain," *Non-Destructive Test.*, vol. 23, no. 10, pp. 424–426, Oct. 2001.
[4] *Application Guide of the Non-Contact Pipeline Magnetic Testing*, 1st ed., The Russian Federation Ore Industry Committee, Moscow, Russia, 2002.
[5] A. A. Dubov and A. Alexander, "Application experience of non-contact magnetometric diagnostics (don't short) of pipelines and perspectives of its development," presented at the 11th ECNDT, Prague, The Czech republic, 2014.
[6] K. X. Liao, Q. Yao, and C. Zhang, "Principle and technical characteristics of non-contact magnetic tomography method inspection for oil and gas pipeline," in *Proc. ICPTT*, Beijing, China, 2011, pp. 1039–1048.
[7] Q. Wan, H. P. Niu, L. M. Wei, L. Sun, and Q. Sh Hu, "Study on nondestructive detection technique of weak magnetic tomography for oil and gas pipelines," *Appl. Math. Mech.*, vol. 35, pp. 221–225, Nov. 2014.
[8] S. S. Kamaeva, I. S. Kolesnikov, and N. A. Eremin, "Remote inspection by the magnetic tomography method (MTM) to prevent the risks imposed by exploitation of Arctic offshore pipelines," presented at the IOP Conf., Mater. Sci. Eng., 2019. [Online]. Available: https://iopscience.iop.org/article/10.1088/1757-899X/700/ 1/012051
[9] R. Jarvis, P. Cawley, and P. B. Nagy, "Performance evaluation of a magnetic field measurement NDE technique using a model assisted probability of detection framework," *NDT & E Int.*, vol. 91, pp. 61–70, Oct. 2017, doi: 10.1016/j.ndteint.2017.06.006.
[10] K. X. Liao, H. Peng, T. J. He, G. X. He, J. H. Leng, and J. H. Zhao, "Non-contact magnetic detection technology and application of ring weld in buried pipe," *Hot Work. Technol.*, vol. 49, no. 23, pp. 111–117, Dec. 2020.
[11] C. Li, C. Chen, and K. Liao, "A quantitative study of signal characteristics of non-contact pipeline magnetic testing," *Insight-Non-Destructive Test. Condition Monit.*, vol. 57, no. 6, pp. 324–330, Jun. 2015, doi: 10.1784/insi.2015.57.6.324.
[12] Y. Han, "Weak magnetic technology and application on pipeline ontology defect testing," *Piping Technol. Equip.*, vol. 3, pp. 27–30, May 2019.
[13] Z. Li, R. Jarvis, P. B. Nagy, S. Dixon, and P. Cawley, "Experimental and simulation methods to study the magnetic tomography method (MTM) for pipe defect detection," *NDT & E Int.*, vol. 92, pp. 59–66, Dec. 2017, doi: 10.1016/j.ndteint.2017.07.018.
[14] R. Osiander, S. A. Ecelberger, and R. B. Givens, "A microelectromechanical-based magnetostrictive magnetometer," *Appl. Phys. Lett.*, vol. 69, pp. 2930–2931, Jun. 1998, doi: 10.1063/1.117327.
[15] N. Sh Chen, Q. Q. Hong, and J. Ch Wang, "Magnetic medium is anisotropic stable current magnetic field," in *Electromagnetic Field for the Anisotropic Medium*, 1st ed. Beijing, China: Science Press, 2012, ch. 2, pp. 155–159.
[16] K. Kiani, "Elastic buckling of current-carrying double-nanowire systems immersed in a magnetic field," *Acta Mechanica*, vol. 227, no. 12, pp. 3549–3570, Dec. 2016, doi: 10.1007/s00707-016-1679-1.
[17] W. C. Zhong, "Why the model of magnetic dipole, but not the model of magnetic domain is used for the research on magnetic testing principle," *Nondestruct. Test.*, vol. 28, no. 2, pp. 94–95, 2006.
[18] Z. Zhang, C. Xiao, J. Gao, and G. Zhou, "Experiment research of magnetic dipole model applicability for a magnetic object," *J. Basic Sci. Eng.*, vol. 18, no. 5, pp. 862–868, 2010, doi: 10.3969/j.issn.1005-0930.2010.05.016.
[19] K. Kiani, "Stability and vibrations of doubly parallel current-carrying nanowires immersed in a longitudinal magnetic field," *Phys. Lett. A*, vol. 379, no. 4, pp. 348–360, Feb. 2015, doi: 10.1016/j.physleta.2014.11.006.
[20] D. F. Wan and X. L. Ma, "Magnetic anisotropy and magnetostriction," in *Magnetophysics*, 1st ed. Beijing, China: PHEI, 1999, ch. 5, pp. 216–269.
[21] K. Kiani and M. Ghaedi, "Vibrational and stability analysis of membrane-like current-carrying nanowires under action of longitudinal magnetic fields," *Eur. Phys. J. Plus*, vol. 135, no. 6, pp. 1–22, Jul. 2020, doi: 10.1140/epjp/s13360-020-00503-8.
[22] K. Keivan, "Vibrations and instability of pretensioned current-carrying nanowires acted upon by a suddenly applied three-dimensional magnetic field," *Mater. Chem. Phys.*, vol. 162, pp. 531–541, Jul. 2015, doi: 10.1016/j.matchemphys.2015.05.080.
[23] B. Q. Chen, Y. S. Shu, and W. Y. Hu, "Electromagnetic properties of matter," in *Special Topics in Electromagnetics*, 1st ed. Beijing, China: HEP, 2001, ch. 4, pp. 243–255.
[24] J. Her-Nan, "Defect characterization by magnetic leakage fields," *Brit. J. NDT*, vol. 19, pp. 132–144, Jan. 1977.
[25] X. Y. Wang and W. J. Li, "Distributing of magnetic field about a current carrying coil," *J. Xi'an Inst. Technol.*, vol. 3, pp. 292–295, Jan. 2004.
[26] L. J. Yang, B. Liu, and S. W. Gao, "Study on magnetic flux leakage testing in weak testing in weak magnetic field," *Instrum. Technique Sensor*, vol. 1, pp. 89–92, Jan. 2014.
[27] Y. Sh Sun, "On the calculating models of permanent magnets," *Acta Electronica Sinica*, vol. 5, pp. 86–89, Sep. 1982.
[28] X. Y. Li, J. W. Xu, and H. J. Liu, "Three-dimensional magnetic field distribution around a rectangular permanent magnet," *J. Beijing Univ. Technol.*, vol. 1, pp. 1–6, Apr. 2008.
[29] A. A. Dubov, A. A. Dubov, and S. M. Kolokolnikov, "Non-contact magnetometric diagnostics of potentially hazardous sections of buried and insulated pipelines susceptible to failure," *Weld. World*, vol. 61, no. 1, pp. 107–115, Nov. 2016, doi: 10.1007/s40194-016-0402-0.
[30] J. Jeon, W. Chung, and H. Son, "Magnetic induction tomography using magnetic dipole and lumped parameter model," *IEEE Access*, vol. 7, pp. 70287–70295, 2019, doi: 10.1109/ACCESS.2019.2919140.
[31] S. Zhang, X. Zhang, H. Wang, M. Zhao, Y. Li, G. Xu, and W. Yan, "Forward solver in magnetoacoustic tomography with magnetic induction by generalized finite-element method," *IEEE Trans. Magn.*, vol. 52, no. 3, pp. 1–4, Mar. 2016, 5100204, doi: 10.1109/TMAG.2015.2480877.
[32] H. Brauer, M. Ziolkowski, M. Kuilekov, S. Men, and C. Resagk, "Surface current reconstruction using magnetic field tomography," *IEEE Trans. Magn.*, vol. 40, no. 2, pp. 1398–1401, Mar. 2004, doi: 10.1109/TMAG.2004.824903.

[33] T. Omori, Y. Takeiri, and B. J. Peterson, "Study on the leakage fields prediction of a static ferromagnetic shield in consideration of hysteresis and residual strain of shielding materials," in *Jpn. J. Appl. Phys.*, vol. 47, p. 3673, May 2008, doi: 10.1143/jjap.47.3673.
[34] K. Yee, "Numerical solution of initial boundary value problems involving Maxwell's equations in isotropic media," *IEEE Trans. Antennas Propag.*, vol. 14, no. 3, pp. 302–307, May 1966, doi: 10.1109/TAP.1966.1138693.
[35] W. Hafla, A. Buchau, F. Groh, and W. M. Rucker, "Efficient integral equation method for the solution of 3-D magnetostatic problems," *IEEE Trans. Magn.*, vol. 41, no. 5, pp. 1408–1411, May 2005, doi: 10.1109/TMAG.2005.844342.
[36] S. Babic, C. Akyel, and M. M. Gavrilovic, "Calculation improvement of 3D linear magnetostatic field based on fictitious magnetic surface charge," *IEEE Trans. Magn.*, vol. 36, no. 5, pp. 3125–3127, Sep. 2000, doi: 10.1109/20.908707.
[37] T. Omori, Y. Takeiri, and B. J. Peterson, "Study on the leakage fields prediction of a static ferromagnetic shield in consideration of hysteresis and residual strain of shielding materials," *Jpn. J. Appl. Phys.*, vol. 47, no. 5, pp. 3673–3681, May 2008, doi: 10.1143/jjap.47.3673.
[38] D. C. Jiles and L. Li, "A new approach to modeling the magnetomechanical effect," *J. Appl. Phys.*, vol. 95, no. 11, pp. 7058–7060, Jun. 2004, doi: 10.1063/1.1687200.
[39] S. Suzuki, T. Kawamata, R. Simura, S. Asano, S. Fujieda, R. Y. Umetsu, M. Fujita, M. Imafuku, T. Kumagai, and T. Fukuda, "Anisotropy of magnetostriction of functional BCC iron-based alloys," *Mater. Trans.*, vol. 60, no. 11, pp. 2235–2244, Nov. 2019, doi: 10.2320/matertrans.MT-M2019146.
[40] Y. S. Li, Q. Z. Liu, J. Liu, and X. J. Tang, "The unit integral calculation method of defective material's forward question of magnetic flux leakage detection based on the magnetic dipole model," *Trans. China Electrotech. Soc.*, vol. 32, no. 21, pp. 176–185, Nov. 2017, doi: 10.19595/j.cnki.1000-6753.tces.170430.
[41] J. C. Compter, J. L. G. Janssen, and E. A. Lomonova, "Ampere's circuital 3-D model for noncuboidal magnets," *IEEE Trans. Magn.*, vol. 46, no. 12, pp. 4009–4015, Dec. 2010, doi: 10.1109/TMAG.2010.2070804.
[42] M. Kan, Z. Zhang, B. Xiao, L. Yang, S. Duan, G. Wang, and G. Wang, "Simulation of magnetically driven flyer plate experiments with an improved magnetic field boundary formula," *High Energy Density Phys.*, vol. 26, pp. 38–43, Mar. 2018, doi: 10.1016/j.hedp.2017.12.002.
[43] N. Demerdash, T. Nehl, and F. Fouad, "Finite element formulation and analysis of three dimensional magnetic field problems," *IEEE Trans. Magn.*, vol. 16, no. 5, pp. 1092–1094, Sep. 1980, doi: 10.1109/TMAG.1980.1060817.
[44] R. Ravaud, G. Lemarquand, S. Babic, V. Lemarquand, and C. Akyel, "Cylindrical magnets and coils: Fields, forces, and inductances," *IEEE Trans. Magn.*, vol. 46, no. 9, pp. 3585–3590, Sep. 2010, doi: 10.1109/TMAG.2010.2049026.
[45] R. Ravaud, G. Lemarquand, and V. Lemarquand, "Magnetic field created by tile permanent magnets," *IEEE Trans. Magn.*, vol. 45, no. 7, pp. 2920–2926, Jul. 2009, doi: 10.1109/TMAG.2009.2014752.

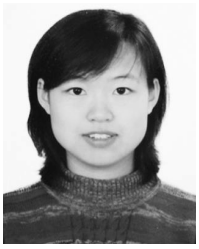

LINLIN LIU received the M.S. degree in control science and engineering from the Beijing University of Chemical Technology, Beijing, China, in 2011. She is currently pursuing the Ph.D. degree with the School of Information Science and Engineering, Shenyang University of Technology, Liaoning, China. Her research interests include magnetic tomography method, magnetic distribution, and nondestructive detection technology and theory of long oil and gas pipeline.

LIJIAN YANG received the M.Sc. degree from the Harbin Institute of Technology, in 1984.

He is currently a Professor and a Doctoral Supervisor with the Shenyang University of Technology. He is the author of two books, more than 100 articles, and more than ten inventions. His research interests include nondestructive testing detection technology and theory of long oil and gas pipeline.

Prof. Yang was a recipient of the Second Prize of National Science and Technology Progress, China, in 2004, and Second Prize of Science and Technology Progress of National Machinery Industry, China, in 2003.

SONGWEI GAO is currently a Professor and a Doctoral Supervisor with the Shenyang University of Technology. Her research interests include nondestructive testing detection technology and theory of long oil and gas pipeline.